Edge preserving smoothing and segmentation of 4-D images via transversely isotropic scale-space processing and fingerprint analysis

Bryan W. Reutter[a,b], V. Ralph Algazi[b], Grant T. Gullberg[a], and Ronald H. Huesman[a]

[a]Nuclear Medicine & Functional Imaging, Lawrence Berkeley National Laboratory
One Cyclotron Road MS55R0121, Berkeley, CA 94720-8119, USA
[b]Center for Image Processing & Integrated Computing
University of California, One Shields Avenue, Davis, CA 95616-8553, USA

ABSTRACT

Enhancements are described for an approach that unifies edge preserving smoothing with segmentation of time sequences of volumetric images, based on differential edge detection at multiple spatial and temporal scales. Potential applications of these 4-D methods include segmentation of respiratory gated positron emission tomography (PET) transmission images to improve accuracy of attenuation correction for imaging heart and lung lesions, and segmentation of dynamic cardiac single photon emission computed tomography (SPECT) images to facilitate unbiased estimation of time-activity curves and kinetic parameters for left ventricular volumes of interest. Improved segmentation of lung surfaces in simulated respiratory gated cardiac PET transmission images is achieved with a 4-D edge detection operator composed of edge preserving 1-D operators applied in various spatial and temporal directions. Smoothing along the axis of a 1-D operator is driven by structure separation seen in the scale-space fingerprint, rather than by image contrast. Spurious noise structures are reduced with use of small-scale isotropic smoothing in directions transverse to the 1-D operator axis. Analytic expressions are obtained for directional derivatives of the smoothed, edge preserved image, and the expressions are used to compose a 4-D operator that detects edges as zero-crossings in the second derivative in the direction of the image intensity gradient. Additional improvement in segmentation is anticipated with use of multiscale transversely isotropic smoothing and a novel interpolation method that improves the behavior of the directional derivatives. The interpolation method is demonstrated on a simulated 1-D edge and incorporation of the method into the 4-D algorithm is described.

Keywords: multiscale 4-D image processing, feature extraction, segmentation

1. INTRODUCTION

Nonlinear edge preserving smoothing is often performed prior to medical image segmentation. The goal of the nonlinear smoothing is to improve segmentation accuracy by preserving significant changes in image intensity while smoothing random noise fluctuations. Methods include median filtering,[1] gray-scale morphology,[2] and spatially varying smoothing driven by local contrast measures[3] or nonlinear diffusion.[4,5] Nonlinear preprocessing can be particularly helpful for segmenting low-contrast images whose edges would be overly blurred by spatially invariant linear smoothing performed in an attempt to achieve a desired contrast to noise ratio.

Rather than irreversibly altering images with edge preserving smoothing prior to segmentation, we have been developing an approach that unifies edge preserving smoothing with segmentation based on differential edge detection at multiple scales.[6,7] Analysis of time sequences of volumetric images (i.e., 4-D data) is decomposed into independent 1-D problems. Smoothing in various directions along 1-D profiles through 4-D data is driven

Further author information: (Send correspondence to B.W.R. at Lawrence Berkeley Laboratory address)
B.W.R.: E-mail: bwreutter@lbl.gov, Telephone: 1 510 486 4265, FAX: 1 510 486 4768
V.R.A.: E-mail: vralgazi@ucdavis.edu, Telephone: 1 530 752 8066, FAX: 1 530 752 8894
G.T.G.: E-mail: gtgullberg@lbl.gov, Telephone: 1 510 486 7483, FAX: 1 510 486 4768
R.H.H.: E-mail: rhhuesman@lbl.gov, Telephone: 1 510 486 4062, FAX: 1 510 486 4768

by a measure of local structure separation seen in the scale-space fingerprint, rather than by a local contrast measure. Analytic expressions are obtained for the derivatives of edge preserved 1-D profiles. Using these expressions, multidimensional edge detection operators such as the Laplacian or the second derivative in the direction of the image intensity gradient are composed and used to segment 4-D data. This previous work is summarized in Sections 2 and 3.

In the present work, we perform additional small-scale isotropic smoothing in directions transverse to each 1-D profile to reduce spurious noise structures without adversely affecting localization of true edges. Improved segmentation results for simulated 4-D medical images are presented in Section 4, along with a mathematical framework for incorporating results of transversely isotropic smoothing at multiple scales. We also report preliminary results of a novel interpolation method that is anticipated to further improve differential edge detection by improving the behavior of the derivatives along the edge preserved 1-D profiles.

Potential applications of these methods include 4-D spatiotemporal segmentation of respiratory gated positron emission tomography (PET) transmission images to improve accuracy of attenuation correction for imaging heart and lung lesions,[8,9] and 4-D spatiotemporal segmentation of dynamic cardiac single photon emission computed tomography (SPECT) images to facilitate unbiased estimation of time-activity curves and kinetic parameters for left ventricular volumes of interest.[10,11]

2. PRESERVING 1-D EDGES VIA RECURSIVE MULTISCALE BLENDING

We use recursive multiscale blending[6,7] to perform nonlinear edge preserving smoothing along 1-D profiles:

$$\tilde{\mathrm{f}}(x, a_j) = \begin{cases} \bar{\mathrm{f}}(x, a_1) & j = 1 \\ [1 - \mathrm{C}_j(x)]\, \tilde{\mathrm{f}}(x, a_{j-1}) + \mathrm{C}_j(x)\bar{\mathrm{f}}(x, a_j) & j = 2, \ldots, J, \end{cases} \tag{1}$$

where $\tilde{\mathrm{f}}(x, a_j)$ is a smoothed, edge preserved version of the 1-D signal $\mathrm{f}(x)$, a_j is a scale parameter, $\mathrm{C}_j(x)$ is a blending function that is constrained to lie between 0 and 1, and J is the total number of scales. The edge preserved signal $\tilde{\mathrm{f}}(x, a_j)$ is a convex combination of the signals $\{\bar{\mathrm{f}}(x, a_i);\ i = 1, \ldots, j\}$, which are linearly smoothed versions of $\mathrm{f}(x)$ obtained via convolution with kernels based on the uniform cubic B-spline basis function.[12–14] The cubic B-spline with scale parameter a_j has a support of $4a_j$ and approximates a Gaussian with standard deviation $\sigma_j = \sqrt{1/3}\, a_j$. Typically, the total number of scales J ranges between 3–5 and dyadic sampling of the scale coordinate a is used so that $a_j = 2^{j-1} a_1$.

The blending functions $\{\mathrm{C}_j(x);\ j = 2, \ldots, J\}$ play a role similar to that of spatially varying diffusion coefficients used in typical implementations of edge preserving smoothing via nonlinear diffusion (e.g., Refs. 4, 5). When $\mathrm{C}_j(x_0) = 0$, smoothing stops in the neighborhood of x_0 and $\tilde{\mathrm{f}}(x_0, a_j)$ remains unchanged from the value $\tilde{\mathrm{f}}(x_0, a_{j-1})$ obtained with use of edge preserving smoothing at the previous, finer scale. When $\mathrm{C}_j(x_0) = 1$, smoothing is unabated and $\tilde{\mathrm{f}}(x_0, a_j)$ is set to the value $\bar{\mathrm{f}}(x_0, a_j)$ obtained with use of linear smoothing at the current, coarser scale.

The blending functions are defined via an analysis of the augmented scale-space fingerprint (Figure 1). At a particular scale, the amount of blending is decreased as the separation between fingerprint lines increases, such as in the neighborhood of edges.[6,7] Figure 2 shows edge preserving smoothing results for the noisy ramp edge shown in Figure 1. Recursive multiscale blending yields a sharper edge than does linear smoothing and provides comparable smoothing away from the edge (Figure 2a). The blending functions consistently reach their minimum near the edge, thus reducing the amount of smoothing in the neighborhood of the edge (Figure 2b). Away from the edge, the blending functions increase, thus increasing the amount of smoothing. Because of the high noise level, the apparent position of the edge is shifted to the right.

With use of Equation (1), an analytic expression can be obtained for the first derivative along a smoothed, edge preserved 1-D profile:

$$\tilde{\mathrm{f}}^{(1)}(x, a_j) = \begin{cases} \bar{\mathrm{f}}^{(1)}(x, a_1) & j = 1 \\ \tilde{\mathrm{f}}^{(1)}(x, a_{j-1}) + \mathrm{C}_j(x) \left[\bar{\mathrm{f}}^{(1)}(x, a_j) - \tilde{\mathrm{f}}^{(1)}(x, a_{j-1})\right] & \\ \qquad + \mathrm{C}_j^{(1)}(x) \left[\bar{\mathrm{f}}(x, a_j) - \tilde{\mathrm{f}}(x, a_{j-1})\right] & j = 2, \ldots, J, \end{cases} \tag{2}$$

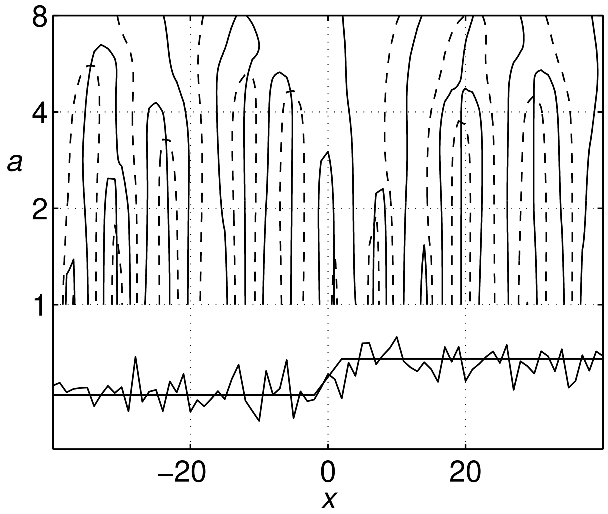

Figure 1. Augmented scale-space fingerprint[14] for a noisy ramp edge of width four and a contrast to noise ratio of 2.5. Solid fingerprint lines depict the zero-crossing locations of the second derivative (i.e., edge locations) over a continuum of scales. Dashed lines depict the zero-crossing locations of the first derivative (i.e., ridge and trough locations). The noiseless edge is shown with the noisy edge below the fingerprint.

where superscripts in parentheses denote the order of derivatives with respect to x. The second derivative along the 1-D profile is

$$\tilde{\mathrm{f}}^{(2)}(x,a_j) = \begin{cases} \bar{\mathrm{f}}^{(2)}(x,a_1) & j=1 \\ \tilde{\mathrm{f}}^{(2)}(x,a_{j-1}) + \mathrm{C}_j(x)\left[\bar{\mathrm{f}}^{(2)}(x,a_j) - \tilde{\mathrm{f}}^{(2)}(x,a_{j-1})\right] & \\ \qquad + 2\mathrm{C}_j^{(1)}(x)\left[\bar{\mathrm{f}}^{(1)}(x,a_j) - \tilde{\mathrm{f}}^{(1)}(x,a_{j-1})\right] & j=2,\ldots,J. \\ \qquad + \mathrm{C}_j^{(2)}(x)\left[\bar{\mathrm{f}}(x,a_j) - \tilde{\mathrm{f}}(x,a_{j-1})\right] & \end{cases} \tag{3}$$

Equation (1) has the desirable property that the nonlinearly smoothed signal $\tilde{\mathrm{f}}(x,a_j)$ is bounded by the extrema of the linearly smoothed signals $\{\bar{\mathrm{f}}(x,a_i);\, i=1,\ldots,j\}$ for all x. However, the derivatives given by Equations (2) and (3) can be less well-behaved and can contain spurious zero-crossings that generate false edges in the output of the multidimensional edge detection operator described in Section 3. The goal of the work described in Section 4 is to reduce these false edges.

3. PRESERVING AND SEGMENTING MULTIDIMENSIONAL EDGES

Edges can be preserved in multidimensional (n-D) image data by applying the 1-D smoothing algorithm described in Section 2 independently along the coordinate axis directions and along the diagonal directions of the 2-D planes spanned by the coordinate axes, and averaging the results. We refer to this as *multidirectional 1-D processing* and note that this builds on work by Weickert *et al*[5] in which processing was performed only along the coordinate axis directions. The information obtained along the diagonal directions allows characterization of first and second order differential properties of the data in any direction.[14] Using this additional information, multidimensional edge detection operators such as the Laplacian or the second derivative in the direction of the image intensity gradient can be composed and used to segment the data as follows.

The n-D data array is denoted by $\mathrm{f}(\mathbf{x})$, where $\mathbf{x} = \begin{bmatrix} x_1 & \cdots & x_n \end{bmatrix}^{\mathrm{T}}$ is the position vector for the domain of the data and "$[\ ]^{\mathrm{T}}$" denotes the matrix transpose. The 1-D profile passing through the point $\mathbf{x}_0$ in the direction $\mathbf{v}_0$ is denoted by

$$\mathrm{f}_{\mathbf{x}_0,\mathbf{v}_0}(s) = \mathrm{f}(\mathbf{x}_0 + s\mathbf{v}_0), \tag{4}$$

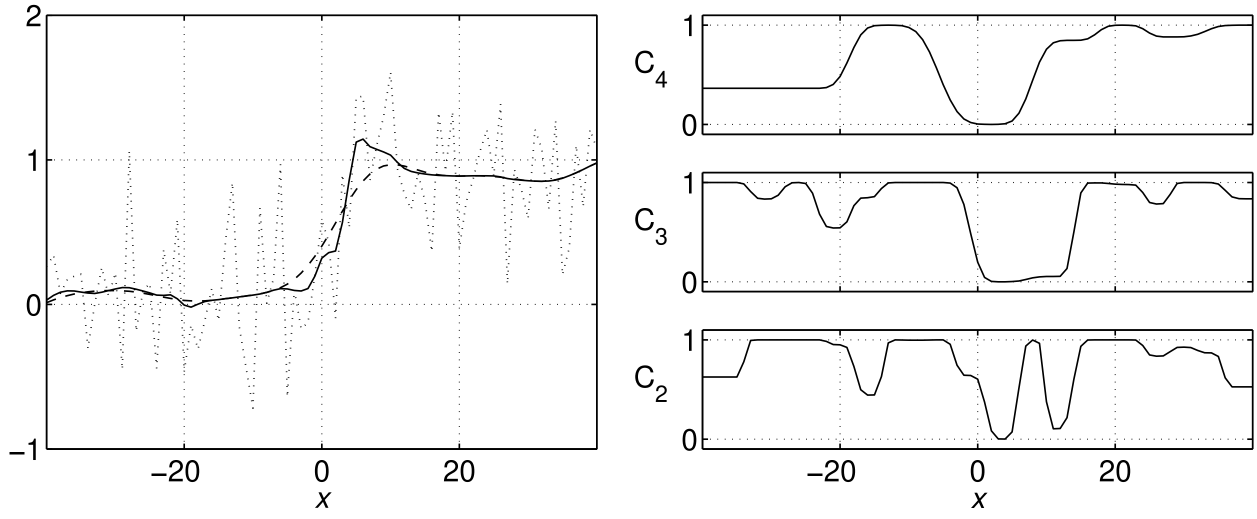

Figure 2. Edge preserving smoothing results for a noisy ramp edge of width four and a contrast to noise ratio of 2.5. In (a), the dashed line and solid line depict linear and nonlinear smoothing results, respectively, at scale $a_4 = 8$. The dotted line depicts the unsmoothed signal, which is also shown in Figure 1 along with its scale-space fingerprint and the noiseless signal. The blending functions $\mathrm{C}_2(x)$, $\mathrm{C}_3(x)$, and $\mathrm{C}_4(x)$ used to perform nonlinear smoothing are shown in (b).

where $\mathbf{v} = \begin{bmatrix} v_1 & \cdots & v_n \end{bmatrix}^{\mathrm{T}}$ is a unit vector and s is an arc length parameter. The relationships between the first and second derivatives of $\mathrm{f}_{\mathbf{x},\mathbf{v}}(s)$ and the first and second order partial derivatives of the n-D data $\mathrm{f}(\mathbf{x})$ are

$$\frac{d\mathrm{f}_{\mathbf{x},\mathbf{v}}}{ds} = \mathbf{v} \cdot \nabla \mathrm{f} = \mathbf{v}^{\mathrm{T}}\mathbf{g} \tag{5}$$

$$\frac{d^2\mathrm{f}_{\mathbf{x},\mathbf{v}}}{ds^2} = \mathbf{v} \cdot \nabla[\mathbf{v} \cdot \nabla \mathrm{f}] = \mathbf{v}^{\mathrm{T}}\mathbf{H}\mathbf{v}, \tag{6}$$

where $\mathbf{g}(\mathbf{x})$ is the image intensity gradient vector and $\mathbf{H}(\mathbf{x})$ is the Hessian matrix. One can rewrite Equation (6) as an inner product of $(\frac{n^2+n}{2})$-element vectors:

$$\frac{d^2\mathrm{f}_{\mathbf{x},\mathbf{v}}}{ds^2} = \mathbf{w}^{\mathrm{T}}\mathbf{h}, \tag{7}$$

where

$$\mathbf{w} = \begin{bmatrix} v_1^2 & 2v_1v_2 & \cdots & 2v_1v_n & v_2^2 & 2v_2v_3 & \cdots & 2v_2v_n & \cdots & v_{n-1}^2 & 2v_{n-1}v_n & v_n^2 \end{bmatrix}^{\mathrm{T}} \tag{8}$$

$$\mathbf{h} = \begin{bmatrix} H_{11} & H_{12} & \cdots & H_{1n} & H_{22} & H_{23} & \cdots & H_{2n} & \cdots & H_{(n-1)(n-1)} & H_{(n-1)n} & H_{nn} \end{bmatrix}^{\mathrm{T}} \tag{9}$$

and $H_{ij} = \frac{\partial^2 \mathrm{f}}{\partial x_i \partial x_j}$. Given derivative estimates in all 1-D profiles along the coordinate axis directions and diagonal directions of 2-D planes spanned by the coordinate axes (for a total of n^2 directions), one can compute least squares estimates of the image intensity gradient vector $\mathbf{g}(\mathbf{x})$ and the vector $\mathbf{h}(\mathbf{x})$ of Hessian matrix elements.[7, 14] Using these estimates one can compose multidimensional operators that detect edges as zero-crossings in the Laplacian, trace($\mathbf{H}$), or in the second derivative in the direction of the gradient, weighted by the squared magnitude of the gradient, $\mathbf{g}^{\mathrm{T}}\mathbf{H}\mathbf{g}$.

4. REDUCING FALSE EDGES

We have been refining the methods described in Sections 2 and 3 to improve 4-D medical image segmentations obtained with use of edge preserving smoothing via multiscale recursive blending. The goal is to reduce noise in the 1-D profile derivatives with minimal additional blurring along the profile, and thereby reduce spurious structures in segmentations without adversely affecting localization of true edges.

4.1. Effects of Small-Scale Transversely Isotropic Smoothing

We used simulated 4-D medical image data to investigate the benefit that results from performing additional small-scale isotropic smoothing with a 3×3×3 kernel in directions transverse to each 1-D profile, prior to recursive multiscale blending. This small-scale transversely isotropic smoothing improved lung surface segmentations in simulated respiratory gated cardiac PET transmission images (Figure 3), compared to segmentations that we obtained previously (Ref. 7, Fig. 2, page 436).

The 4-D image array was generated with use of the Mathematical Cardiac Torso (MCAT) software phantom[15] and was composed of 40 contiguous 5 mm-thick transverse slices at 15 respiratory phases. Figure 3a shows a 3-D wireframe rendering of the known lung surface segmentation at respiratory phase 8. Each transverse slice had 80×80 pixels with pixel size 5 mm × 5 mm. Diaphragm and heart motion of 15 mm in the superior-inferior direction was simulated, in conjunction with chest wall diameter changes of 9.8 mm in the left-right direction and 20 mm in the anterior-posterior direction. Gaussian white noise was added to the images to yield contrast to noise ratios of 5.0 at the air-soft tissue boundary and 3.5 at the soft tissue-lung boundaries (Figure 3b).

Subsequent to small-scale transversely isotropic smoothing, linear 1-D filtering at $J = 3$ scales and recursive multiscale blending were applied independently along the x, y, z, and t axes of the noisy 80×80×40×15 dataset and along the 12 diagonal directions of the 2-D planes spanned by the axes. The longest 1-D linear filter had a support of 19 pixels and approximated a Gaussian with $\sigma = \sqrt{6}$ pixels. For comparison, linear smoothing was also performed on the original noisy data with use of a 7×7×7×7 separable filter that approximated a 4-D Gaussian with $\sigma = 1.1$ pixels. This separable filter yielded the same noise reduction for independent, identically distributed Gaussian noise as that obtained by averaging the outputs of the sixteen 1×19 linear 1-D smoothing filters. Edge preserved results were generated by averaging the outputs of the sixteen 1×19 nonlinear 1-D smoothing filters obtained with use of recursive multiscale blending.

Visual differences were subtle between the smoothed images, which had substantially reduced noise because of the smoothing performed in all four spatial and temporal dimensions (Figures 3d,f,h). Differences were evident, however, between segmentations obtained with 4-D operators that detected edges as zero-crossings in the second derivative in the direction of the image intensity gradient (Figures 3c,e,g). Lung surfaces were detected fairly accurately by the 7×7×7×7 separable operator, but the segmentation also contained many spurious noise structures, as seen in the 3-D wireframe rendering of extracted surfaces in Figure 3c and the display of surface cross sectional contours on the smoothed image in Figure 3d. In particular, noise structures extended outside the lungs throughout the chest wall and mediastinum. Noise structures were reduced by processing with the linear 16×(1×19) operator (Figure 3e), but localization of lung surfaces was inaccurate (Figure 3f) because of the long support of the 1-D linear filters. The edge preserving 16×(1×19) operator restored the accuracy of lung surface localization without unduly increasing spurious noise structures (Figures 3g,h).

4.2. Recursive Blending of Results of Multiscale Transversely Isotropic Smoothing

When transversely isotropic smoothing is performed at multiple scales, Equation (1) can be generalized so that the edge preserved signal $\tilde{\mathrm{f}}(x, a_j)$ is a convex combination of the signals $\{\bar{\mathrm{f}}(x, a_i, b_k);\ i = 1, \ldots, j;\ k = 1, \ldots, K\}$, where $\bar{\mathrm{f}}(x, a_j, b_k)$ is a 1-D profile through n-D data that have smoothed with a kernel having scale parameter a_j in the direction parallel to the profile and scale parameter b_k in the $(n-1)$ dimensions transverse to the profile. We refer to a_j as the *longitudinal scale parameter* and to b_k as the *transverse scale parameter*. The generalization of Equation (1) is

$$\tilde{\mathrm{f}}(x, a_j) = \begin{cases} \displaystyle\sum_{k=1}^{K} \mathrm{D}_{1k}(x)\bar{\mathrm{f}}(x, a_1, b_k) & j = 1 \\ \displaystyle[1 - \mathrm{C}_j(x)]\,\tilde{\mathrm{f}}(x, a_{j-1}) + \sum_{k=1}^{K} \mathrm{D}_{jk}(x)\bar{\mathrm{f}}(x, a_j, b_k) & j = 2, \ldots, J, \end{cases} \tag{10}$$

where the blending functions $\{\mathrm{D}_{jk}(x);\ j = 1, \ldots, J;\ k = 1, \ldots, K\}$ are constrained to lie between 0 and 1, $\mathrm{C}_j(x)$ is the sum $\sum_{k=1}^{K} \mathrm{D}_{jk}(x)$, and K is the total number of transverse scales. The blending functions are also subject to the constraints $\sum_{k=1}^{K} \mathrm{D}_{1k}(x) = 1$ and $\sum_{k=1}^{K} \mathrm{D}_{jk}(x) \le 1$ for $j = 2, \ldots, J$. Thus, Equation (1) corresponds to

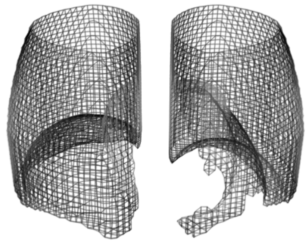

(a) simulated lung surfaces

(b) original noisy image

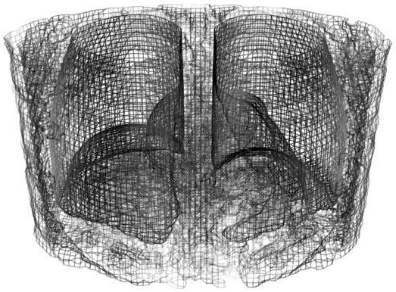

(c) 7×7×7×7 linear smoothing

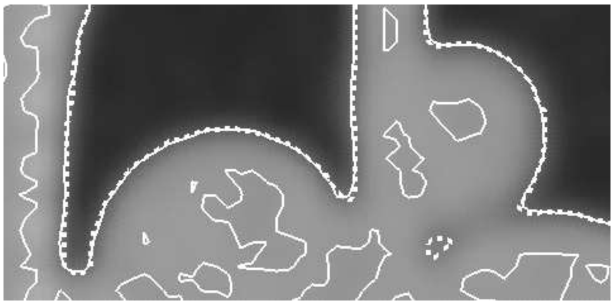

(d) 7×7×7×7 linear smoothing

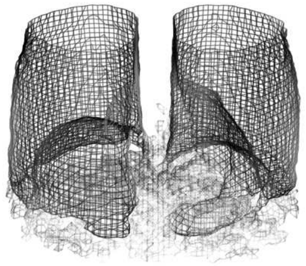

(e) 16×(1×19) linear smoothing

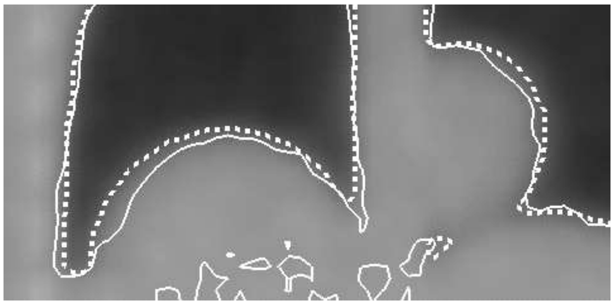

(f) 16×(1×19) linear smoothing

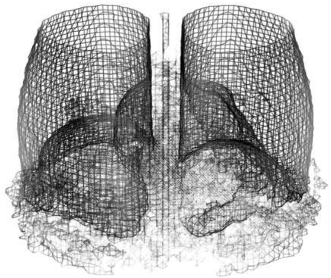

(g) 16×(1×19) edge preserving smoothing

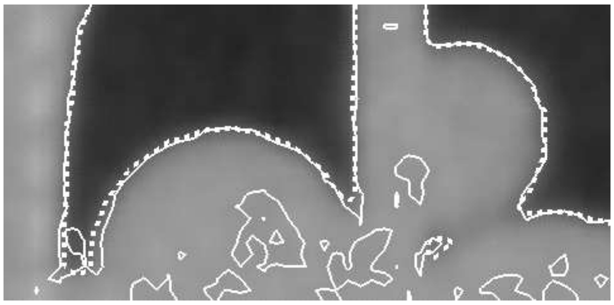

(h) 16×(1×19) edge preserving smoothing

Figure 3. Smoothing and segmenting simulated 4-D respiratory gated PET transmission images. (a) Anterior coronal view of 3-D wireframe rendering of known segmentation of lung surfaces at respiratory phase 8. (b) Noisy 52×26 pixel sub-image from a coronal cross section. The right dome of the diaphragm is the larger, semicircular structure on the left. The heart is the smaller, circular structure on the right. (c,e,g) Wireframe 3-D surface renderings of lung segmentation results for 4-D separable, multidirectional 1-D linear, and multidirectional 1-D edge preserving smoothing, respectively. (d,f,h) Cross sectional contours from surface segmentations shown in (c,e,g), respectively, are depicted as solid lines on smoothed coronal images. Dotted lines depict the true soft tissue-lung boundaries shown in (a).

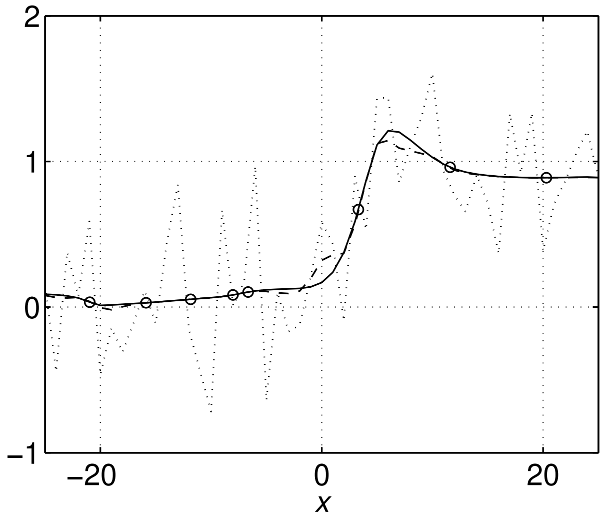

Figure 4. Improving the behavior of the derivatives of an edge preserved 1-D profile. The dashed line depicts the edge preserved profile shown as a solid line in Figure 2a. The solid line in this figure depicts the profile obtained by interpolating the zeroth, first, and second derivatives at the points shown as circles. The well-behaved interpolation removes inflections associated with noise while preserving the inflection associated with the edge.

the case where $K = 1$ and $b_1 = 0$ pixels, and the results presented in Section 4.1 correspond to the case where $K = 1$ and $b_1 = 1$ pixel.

4.3. Improving the Behavior of 1-D Profile Derivatives

We anticipate that the localization accuracy of differential edge detection will be increased and that noise structures will be reduced by improving the behavior of the derivatives along edge preserved 1-D profiles. We have generalized Stineman's interpolation method[16] so that we can interpolate the zeroth, first, and second derivatives at key points along a profile and obtain derivatives with fewer spurious zero-crossings between interpolation points.[17] These refined descriptions of edge preserved profile derivatives will then serve as inputs to the multidimensional edge detection operator.

Figure 4 shows the results of interpolating the zeroth, first, and second derivatives at key points along the edge preserved profile shown in Figure 2a. Our interpolation method removes inflections associated with noise while preserving the inflection associated with the true edge. At a particular scale a_j, interpolation points (depicted as circles in Figure 4) are selected as the intersections of the edge preserved signal at the previous scale, $\tilde{\mathrm{f}}(x, a_{j-1})$, and the linearly smoothed signal at the current scale, $\overline{\mathrm{f}}(x, a_j)$. Equations (1)–(3) are then evaluated at the intersection points to obtain the values to be interpolated. As seen in Figure 4, the intersections include the point where the preserved edge crosses a linearly blurred version of the edge. This intersection occurs near the inflection associated with the edge. Interpolating the relatively large-magnitude first derivative and relatively small-magnitude second derivative at this point preserves the edge.

The interpolation has the added benefit of providing a compact representation of the edge preserved 1-D profile. For example, the 50-pixel segment shown in Figure 4 is analytically described by the values of the zeroth, first, and second derivatives at only 10 points (the 8 points depicted as circles and the next interpolation point lying off of either end).

5. FUTURE DIRECTIONS

The computer simulation in Section 4.1 demonstrates the benefit of performing small-scale isotropic smoothing in directions transverse to each 1-D profile, prior to recursive multiscale blending. Spurious structures in the 4-D image segmentation are reduced without adversely affecting the localization of true edges. Although performed serially here, the computations can be massively parallelized.

In addition to implementing well-behaved interpolation along 1-D profiles through 4-D data as described in Section 4.3, we are investigating the benefit of performing transversely isotropic smoothing at multiple scales as proposed in Section 4.2. We will analyze the properties of the scale-space fingerprint for a 1-D profile as functions of both the longitudinal scale a_j, which controls smoothing along the profile, and the transverse scale b_k, which controls smoothing in directions transverse to the profile. The goal of this fingerprint analysis will be to determine blending functions $\mathrm{D}_{jk}(x)$ for Equation (10) that provide the best compromise between noise reduction and 4-D segmentation accuracy.

ACKNOWLEDGMENTS

The authors thank Dr. Benjamin Tsui at Johns Hopkins University for making the MCAT software phantom available.

This work was supported by the National Heart, Lung, and Blood Institute of the US Department of Health and Human Services under grant R01-HL50663 and by the Director, Office of Science, Office of Biological and Environmental Research, Medical Sciences Division of the US Department of Energy under contract DE-AC03-76SF00098. This work was developed in part with use of resources at the US Department of Energy National Energy Research Scientific Computing (NERSC) Center.

REFERENCES

1. A. K. Jain, *Fundamentals of Digital Image Processing*, Prentice-Hall, Englewood Cliffs, 1989.
2. S. R. Sternberg, "Grayscale morphology," *Comput. Vis. Graph. Image Proc.* **35**(3), pp. 333–355, 1986.
3. K. Kitamura, H. Iida, M. Shidahara, S. Miura, and I. Kanno, "Noise reduction in PET attenuation correction using non-linear Gaussian filters," *IEEE Trans. Nucl. Sci.* **47**(3), pp. 994–999, 2000.
4. J. Weickert, "A review of nonlinear diffusion filtering," in *Scale-Space Theory in Computer Vision: Proceedings of the First International Conference*, B. T. Haar Romeny, L. Florack, J. Koenderink, and M. Viergever, eds., *Lecture Notes in Computer Science* **1252**, pp. 3–28, 1997.
5. J. Weickert, B. M. T. Haar Romeny, and M. A. Viergever, "Efficient and reliable scheme for nonlinear diffusion filtering," *IEEE Trans. Image Proc.* **7**(3), pp. 398–410, 1998.
6. B. W. Reutter, V. R. Algazi, and R. H. Huesman, "Computationally efficient nonlinear edge preserving smoothing of n-D medical images via scale-space fingerprint analysis," in *2000 IEEE Nuclear Science Symposium and Medical Imaging Conference Record*, D. Merelli, J. Surget, and M. Ulma, eds., pp. 15/282–286, 2001.
7. B. W. Reutter, V. R. Algazi, and R. H. Huesman, "Nonlinear edge preserving smoothing and segmentation of 4-D medical images via scale-space fingerprint analysis," in *Information Processing in Medical Imaging: Proceedings of the Seventeenth International Conference*, M. F. Insana and R. M. Leahy, eds., *Lecture Notes in Computer Science* **2082**, pp. 431–437, 2001.
8. B. W. Reutter, G. J. Klein, and R. H. Huesman, "Automated 3-D segmentation of respiratory-gated PET transmission images," *IEEE Trans. Nucl. Sci.* **44**(6), pp. 2473–2476, 1997.
9. S. A. Nehmeh, Y. E. Erdi, C. C. Ling, K. E. Rosenzweig, H. Schoder, S. M. Larson, H. A. Macapinlac, O. D. Squire, and J. L. Humm, "Effect of respiratory gating on quantifying PET images of lung cancer," *J. Nucl. Med.* **43**(7), pp. 876–881, 2002.
10. B. W. Reutter, G. T. Gullberg, and R. H. Huesman, "Kinetic parameter estimation from dynamic cardiac patient SPECT projection measurements," in *1998 IEEE Nuclear Science Symposium and Medical Imaging Conference Record*, R. Sudharsanan, ed., pp. 1953–1958, 1999.
11. B. W. Reutter, G. T. Gullberg, and R. H. Huesman, "Direct least-squares estimation of spatiotemporal distributions from dynamic SPECT projections using a spatial segmentation and temporal B-splines," *IEEE Trans. Med. Imag.* **19**(5), pp. 434–450, 2000.
12. M. Unser, A. Aldroubi, and M. Eden, "The L_2 polynomial spline pyramid," *IEEE Trans. Patt. Anal. Mach. Intell.* **15**(4), pp. 364–379, 1993.
13. Y.-P. Wang and S. L. Lee, "Scale-space derived from B-splines," *IEEE Trans. Patt. Anal. Mach. Intell.* **20**(10), pp. 1040–1055, 1998.

14. B. W. Reutter and V. R. Algazi, "Computationally efficient anisotropic scale-space processing of 4-D medical images," Tech. Rep. LBNL-42584, Lawrence Berkeley National Laboratory, 1998.
15. W. P. Segars, D. S. Lalush, and B. M. W. Tsui, "Modeling respiratory mechanics in the MCAT and spline-based MCAT phantoms," *IEEE Trans. Nucl. Sci.* **48**(1), pp. 89–97, 2001.
16. R. W. Stineman, "A consistently well-behaved method of interpolation," *Creative Computing* **6**(7), pp. 54–57, 1980.
17. B. W. Reutter, "Well-behaved interpolation of higher-order derivatives via generalization of Stineman's rational polynomial method," in preparation.

DISCLAIMER